Spectral shapes of Ar-broadened HCl lines in the fundamental band by classical molecular dynamics simulations and comparison with experiments

H. Tran and J.-L. Domenech

Citation: The Journal of Chemical Physics **141**, 064313 (2014); doi: 10.1063/1.4892590
View online: http://dx.doi.org/10.1063/1.4892590
View Table of Contents: http://scitation.aip.org/content/aip/journal/jcp/141/6?ver=pdfcov
Published by the AIP Publishing

Spectral shapes of Ar-broadened HCl lines in the fundamental band by classical molecular dynamics simulations and comparison with experiments

H. Tran[1,a)] and J.-L. Domenech[2]
[1]*Laboratoire Interuniversitaire des Systèmes Atmosphériques, UMR CNRS 7583, Université Paris Est Créteil, Université Paris Diderot, Institut Pierre-Simon Laplace, 94010 Créteil Cedex, France*
[2]*Instituto de Estructura de la Materia, Consejo Superior de Investigaciones Cientificas, (IEM-CSIC), Serrano 123, 28006 Madrid, Spain*

(Received 3 July 2014; accepted 28 July 2014; published online 14 August 2014)

Spectral shapes of isolated lines of HCl perturbed by Ar are investigated for the first time using classical molecular dynamics simulations (CMDS). Using reliable intermolecular potentials taken from the literature, these CMDS provide the time evolution of the auto-correlation function of the dipole moment, whose Fourier-Laplace transform leads to the absorption spectrum. In order to test these calculations, room temperature spectra of various lines in the fundamental band of HCl diluted in Ar are measured, in a large pressure range, with a difference-frequency laser spectrometer. Comparisons between measured and calculated spectra show that the CMDS are able to predict the large Dicke narrowing effect on the shape of HCl lines and to satisfactorily reproduce the shapes of HCl spectra at different pressures and for various rotational quantum numbers. © *2014 AIP Publishing LLC*. [http://dx.doi.org/10.1063/1.4892590]

I. INTRODUCTION

Because of its simple structure, large dipole moment and large rotational constant, HCl is of fundamental interest in the study of intermolecular interactions and is a good system to test the different line-shape models for isolated transitions. Non-Voigt effects on the shape of vibration-rotation lines of HCl have been observed for years (e.g., Refs. 1–7). The large Dicke narrowing effect on the spectra of HCl lines was reported for the first time by Wegdam and Sondag[7] who showed that, at some pressures, the observed width of the 1-0 P(15) line is significantly smaller than its Doppler width. Rao and Oka[4] observed similar phenomena for several lines of the 1-0 band of HCl diluted in Ar. In Refs. 3 and 7, asymmetries of the line shape were also observed. In order to take into account the deviation of the line shape of HCl from the Voigt profile, various models were used. In Refs. 1–3 and 6 the hard[8,9]- and/or soft[10]-collision models were adopted to fit measured spectra of self-, Ar-, N_2-, and air-broadened HCl. It was shown that these models led to much better fits of measured spectra than the Voigt profile. However, the retrieved narrowing parameter, characterizing the spectral effects of the collision-induced translational-velocity changes (i.e., Dicke narrowing effect) strongly depended on the rotational quantum number[2,3] and led to a diffusion coefficient significantly different from the measured value.[1] The impact of the line-narrowing effect on the atmospheric HCl vertical profile, retrieved from ground-based Fourier Transform measurements, was also investigated using the soft-collision model.[11] It was shown that the latter leads to HCl profiles which are in better agreement with independent measurements than those obtained using the Voigt model.[11] More recently, in Ref. 7, a plethora of line-shape models were used to fit measured spectra of N_2- and rare gases-broadened HCl lines: the soft- and hard-collision models; the RGP model which is a combination of hard and soft collision ones; the partially correlated hard-collision model[12,13] taking into account the correlation between velocity- and internal state-changing collisions; the speed-dependent Voigt model[14,15] where the Lorentz width and shift depend on the molecule translational speed; the convolution of the hard- or soft-collision profile with a weighted-sum of Lorentzians,[16,17] the partially correlated speed-dependent Rautian-Sobel'man profile.[13,18] The authors concluded that the best adapted model strongly depends on the pressure, on the considered line and on the perturber and that "*a clear discrimination between all the collisional processes which contribute to the line shape is not possible.*"

In order to understand the different mechanisms affecting the absorption shape of HCl lines, measurement-independent theoretical development must therefore be performed. In recent years, classical molecular dynamics simulations (CMDS) have been successfully used to predict the line shapes of linear molecules such as CO_2 or O_2 without use of any adjustable parameter.[19–22] From reliable intermolecular potentials, one can calculate the auto-correlation function of the dipole moment and then the absorption spectrum. Using a requantization procedure for the classical molecular rotation, the spectrum of a line can be calculated and then compared with the measured profile. As detailed in Ref. 19 for instance, various collision-related effects affecting the shape of an isolated line are taken into account in the calculation. Comparison between CMDS-calculated spectra and measurements for both CO_2 and O_2 absorption lines at different pressures and in

a)Author to whom correspondence should be addressed. Electronic mail: ha.tran@lisa.u-pec.fr

various spectral regions showed very good agreement.[19–22] In the present work, CMDS are thus used for the calculation of the absorption line shapes of HCl diluted in Ar. For that, a new requantization procedure has been adopted in order to represent the rotational motion of HCl molecules. The spectral shape has been computed for different lines of HCl in Ar, from low to relatively high rotational quantum number and for a large range of pressure. High-resolution spectra of several lines of HCl diluted in Ar have also been recorded at various pressures using a difference-frequency laser spectrometer. Comparisons between the CMDS-calculated spectra and these new measurements, and also with those available in the literature, are then made showing a very satisfactory agreement.

This paper is organized as follows: the experimental set-up and the analysis procedure are presented in Sec. II. Section III is devoted to the description of the classical molecular dynamics simulations performed in this work. Comparisons between measured line shapes and CMDS calculations are presented in Sec. IV. Some conclusions and perspectives of this study are summarized in Sec. V.

II. EXPERIMENTAL DETAILS

A. Experimental set-up

Spectra were recorded with the difference-frequency laser spectrometer at IEM-CSIC. This spectrometer is based on the design of Pine[23] and has been often described (see, e.g., Ref. 24), so only a very brief description is given here. Narrow linewidth (0.0001 cm^{-1} full width at half maximum – FWHM) tunable infrared radiation is generated by mixing, in a temperature stabilized $LiNbO_3$ crystal, the radiations from an Ar^+ laser working at 514 nm and a tunable ring dye laser operated with rhodamine 6G. Both lasers run single mode and are actively frequency stabilized, and, in our setup, the Ar^+ laser is also locked to an I_2 hyperfine transition, in order to avoid frequency drifts and to have a well known frequency reference.[25] The infrared beam is split into two paths, one going through the sample cell and to an InSb photodiode and another going directly to a similar InSb detector in order to compensate IR power fluctuations. The Ar^+ laser and, correspondingly, the IR radiation are amplitude modulated at 23 kHz, so we use lock-in amplifiers to obtain the rms value of the photocurrent generated in the detectors due to the mixing process. The wavenumber of the ring dye laser is measured with a solid state wavemeter which makes an instantaneous reading of the frequency in just 1 ms with 10 MHz absolute accuracy, and 3 MHz precision. The wavemeter is calibrated with the frequency-locked Ar^+ laser. The ring dye laser scans 1 cm^{-1} wide segments at 0.01 cm^{-1}/s, and the lock-in time constant is 10 ms at −6 dB/octave roll-off. These conditions ensure that at the lowest pressure and frequency, one Doppler FWHM is scanned in more than 60 time constants, so that instrumental distortions due to scan speed effects are negligible.

The lockin amplifiers outputs, together with other instrumental variables, are digitized at 20 Hz rate in a digital to analog board connected to a PC, which synchronously queries the wavemeter at every data point for the wavenumber of the dye laser. The IR frequency scale is calculated simply by subtracting this wavenumber from that of the Ar^+ laser. The accuracy and precision of the IR frequency scale are limited by those of the ring dye laser. The IR radiation linewidth is that of the convolution of those of the ring and Ar^+ laser, and is also limited by the latter, i.e., $\sim 10^{-4}$ cm^{-1} ($\sim$3 MHz).

The Ar gas was supplied by Air Liquide and the HCl by Praxair, and both had 99.9995% purity, so they were used without further purification. The mixtures were prepared in a steel cylinder generally one day before the experiments to allow for sufficient time for the gases to mix. The concentration was approximately 0.5% of HCl in Ar (40 mbar HCl in $\sim$9 bar total pressure), in order to have a low self-broadening contribution. Given the adsorption/desorption processes of HCl in the cell and cylinder walls, and the lack of an accurate high pressure gauge, the actual partial pressure of HCl was deduced in each spectrum from the observed integrated absorption intensity. The pressure inside the cell was measured continuously during the experiment with two heated capacitance manometers with 1000 and 100 Torr full scale, respectively, and accuracy better than 0.5% of the full scale value.

Measurements were made at room temperature (between 25 and 26 °C). Three cells with different pathlength were used, in order to account for the more than two orders of magnitude difference in intensity between the R(3) and R(11) lines. They have stainless steel or monel bodies and CaF_2 or KBr windows sealed with halocarbon wax, all quite inert to dry HCl. The measurement routine for each line was as follows: first an empty cell spectrum was recorded, then the cell was filled at the highest pressure in the sequence and a spectrum was recorded, then gas was pumped out down to the next pressure and a new spectrum was obtained, and so on, until a new final empty cell spectrum was recorded. For some of the lines another empty cell spectrum was taken in between the sequence. First the signal and reference channels of each spectrum were divided in order to compensate the IR power fluctuations along the scan. The resulting traces had signal-to-noise ratios in excess of 2000. Although all optical elements in the IR path are either tilted or wedged, interference fringes were unavoidable, so all traces in a given sequence were compared paying very special attention to the baseline stability, since small temperature drifts can shift slightly the position of those fringes. Sequences that showed a change in the baseline between traces larger than 3% of the full scale or sequences with a less than a 3% change but where the change did not show a clear and smooth evolution with time were disregarded and repeated. Then for each pressure an empty cell spectrum was calculated as an interpolation according to the elapsed time between the smoothed first and last empty cell traces in the series (if the change between both was at the noise level, this interpolation was avoided). Finally, transmission traces were obtained by dividing each trace by the corresponding empty cell spectrum and then converted to napierian absorbance. Note that fringes have a period of less than 1 cm^{-1}, so the smoothing of the traces is of no consequence for their shape and avoids the factor of 2 degradation of the S/N in the transmission trace. In all cases residual baseline fluctuations are well below the 0.5% level. The measured

TABLE I. Resume of the experimental conditions for the lines recorded. Uncertainties in pathlength and temperature are $\pm 3\sigma$ estimations.

Line	Frequency (cm^{-1})	Pressures (atm)	Pathlength (mm)	Temperature (K)
R(3)	2963.285	0.0066, 0.0132, 0.0263, 0.0392, 0.0526, 0.0643, 0.0928, 0.1329, 0.2550, 0.6628, 0.9207	10 ± 0.5	298 ± 1
R(5)	2998.046	0.0133, 0.0264, 0.0399, 0.0530, 0.0658, 0.0803, 0.1328, 0.2645, 0.3946, 0.6536	10 ± 0.5	298 ± 1
R(7)	3030.087	0.0132, 0.0395, 0.0658, 0.0788, 0.0922, 0.1184, 0.1579, 0.2625, 0.3937, 0.6582	10 ± 0.5	299 ± 1
R(9)	3059.316	0.0263, 0.0527, 0.0796, 0.1181, 0.1572, 0.1970, 0.2641, 0.3947, 0.5266, 0.7881, 0.9149	24.2 ± 0.5	298 ± 1
R(11)	3085.649	0.0525, 0.0926, 0.1316, 0.1580, 0.1842, 0.2117, 0.2607, 0.3905, 0.5261, 0.6562, 0.8391	992 ± 2	299 ± 1

transitions and the corresponding experimental conditions are listed in Table I.

B. Data analysis

The measured spectra have been first least-squares fitted one-by-one by the usual Voigt profile (VP). In order to take into account the non-Voigt behaviour of this system, and as a test, the quadratic-Speed-Dependent Hard-Collision (qSDHC) model is also used to fit the measured spectra. This profile accounts for the Dicke narrowing effect through the hard-collision model[8,9] and for the speed dependence of the collisional width and shift by using the quadratic-dependence law of Refs. 26 and 27. Details of the functional form and parameters characterizing this model can be found in various studies (e.g., Refs. 28–30). Note that in Refs. 31 and 32 it was shown that this profile can be easily computed using the complex probability function.[33]

Figure 1 presents an example of the measured spectra and the corresponding fit residuals using the two models: Voigt profile and quadratic-Speed-Dependent Hard-Collision profile. For each spectrum, the line position including the line shift ($\sigma_0 + \Delta$), the integrated intensity (S), the line width (Γ_0), and its speed dependence (Γ_2), the Dicke narrowing parameter ν_{VC} were retrieved using the qSDHC profile while only $\sigma_0 + \Delta$, S, and Γ (the Lorentz width) were fitted with the Voigt profile. A linear base line was also adjusted together with these parameters. The Doppler width was fixed to its theoretical value, computed from the temperature of the measurement. Note that the speed dependence of the line-shift was neglected in the fits using the qSDHC model. As can be observed in Fig. 1, the Voigt profile leads to large deviations with respect to the measured spectra, with the amplitude of the residual up to more than 10% of the peak absorption. The usual W-shapes observed in the residual (obs − calc) show that the Voigt profile is broader than the measured one. When the qSDHC model is used to fit the measured spectra, a very good agreement is obtained, the residual being almost within the experimental noise. For all considered lines, no asymmetry of the residual can be observed showing that the speed dependence of the line shift is small. Note that although its fit residuals are very small, the qSDHC profile may not be the best adapted model to represent the line shapes of HCl in Ar. Indeed, this model uses simplified approximations (hard collision for velocity-changes effect and quadratic-speed-dependence law for the collisional line

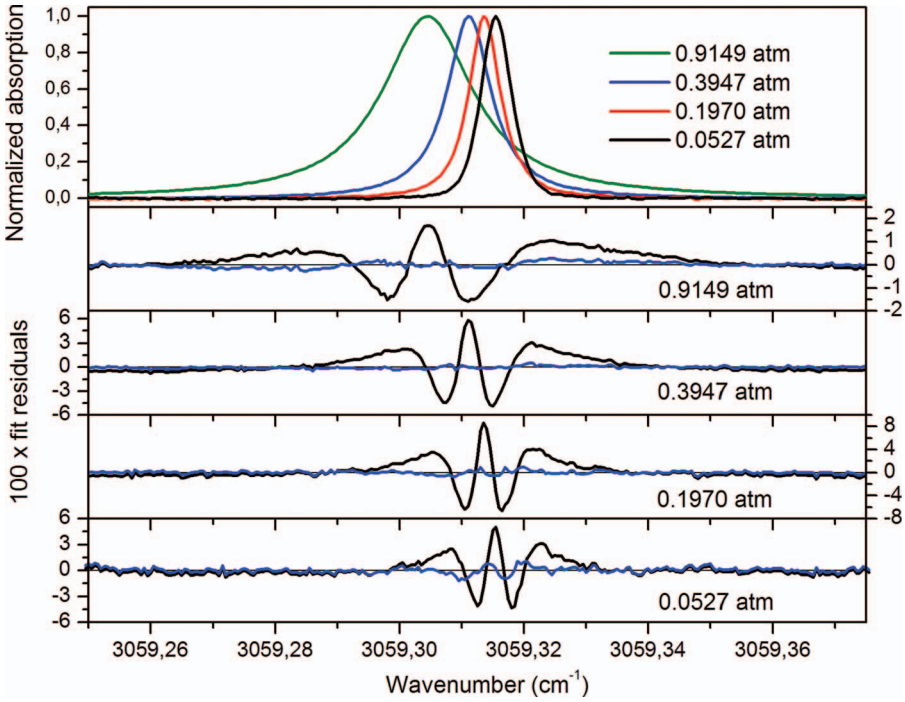

FIG. 1. Peak normalized absorption spectra of HCl diluted in Ar for the R(9) line of the fundamental band, measured at different conditions of pressure (top panel). In the lower panels are the residuals obtained by fitting these spectra with Voigt profiles (black lines) and with the qSDHC profile (blue lines).

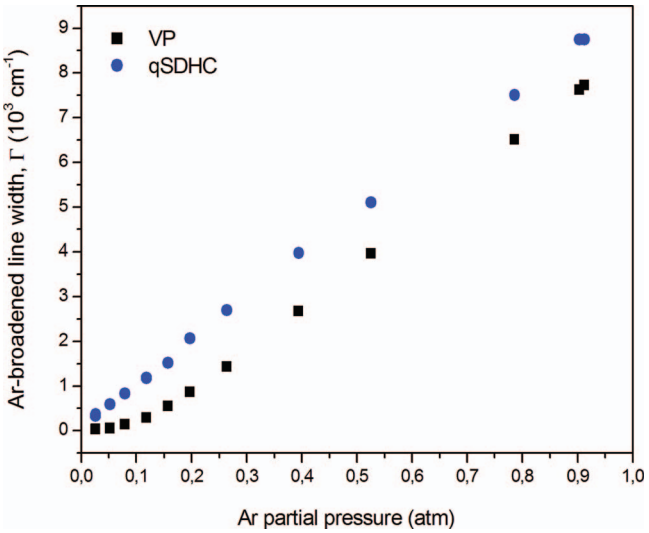

FIG. 2. Ar-broadened width of the 1-0 R(9) line of HCl versus Ar pressure, retrieved from measured spectra using the Voigt profile (black squares) and the quadratic-Speed-Dependent Hard-Collision model (blue circles).

width) and neglects eventual correlation between velocity- and state-changing collisions.

In order to take into account any gas adsorption and/or desorption from the walls of the cell, the concentration of HCl in the mixture is re-determined from the ratio of the retrieved integrated intensity to that given in HITRAN.[34] The Ar-broadened HCl line width is then deduced by subtracting from the retrieved collisional line width the self-broadened part using data of Ref. 34 and the partial pressure of HCl. Figure 2 shows the comparison between the collisional line width (Γ) obtained from fit of measured spectra using the Voigt profile and the qSDHC model. As can be observed, the value of Γ retrieved from measured spectra using the Voigt profile is non linear with the partial pressure of Ar, as opposed to the case where the qSDHC model is used to fit the measured spectra. This can be explained by the non-Voigt shape of the measured profiles (Fig. 1), especially in the Dicke regime where the collisional and the Doppler widths have values close to each other. In order to deduce the broadening coefficient γ ($\gamma = \Gamma/P$) retrieved with the Voigt profile, only values obtained at high pressure (where the Dicke narrowing effect is small) are taken into account. For the qSDHC model, a linear fit of the collisional line width versus pressure directly gives the corresponding broadening coefficient.

Table II and Figure 3 present the values of the broadening coefficient of the considered lines obtained with the two models. The measured line shift, being the same for the two profiles and in good agreement with previous measurements (see Ref. 35 and references therein), is also reported in Table II. Values of existing measured and calculated broadening coefficients are also reported. As expected, the broadening retrieved from the Voigt profile is always smaller than that obtained by the qSDHC profile. This behaviour of the broadening obtained with VP, observed for years for different molecular systems (e.g., Ref. 31 and references therein), indeed is the result of the fitting procedure trying to compensate the fact that the Voigt profile is broader than the experimental one. A good

TABLE II. Ar-broadening coefficient of HCl of the considered lines in the 1-0 band, retrieved from the fit of measured spectra using the Voigt profile and the qSDHC model. (a), (b), (c), (d), and (e) are measured values from Refs. 35, 51–53, and 4, respectively. γ_{CC}^{calc} and γ_{NG}^{calc} are calculated values obtained by close-coupling calculations[36] and by the Neilson and Gordon classical formalism,[35] respectively. The Ar-shifting coefficient measured in this work is presented in last column. All values are in 10^{-3} cm^{-1}/atm.

Line	γ_{VP}^{exp} (this work)	γ_{qSDHC}^{exp} (this work)	Previous γ^{exp}	γ_{CC}^{calc}	γ_{NG}^{calc}	δ^{exp}
R(3)	28.70	29.25	32.0[(a)], 28.87[(b)], 39.51[(c)], 28.05[(d)]	29.4	28.4	− 9.75
R(5)	21.03	21.74	24.2[(a)], 20.67[(b)], 24.82[(c)], 21.63[(d)]	22.3	20.4	− 11.15
R(7)	13.63	15.21	16.6[(a)], 13.98[(b)], 16.71[(c)]	15.6	13.5	− 12.41
R(9)	8.47	9.68	11.1[(a)], 11.14[(c)], 8.77[(e)]		8.8	− 13.07
R(11)	4.42	6.32	8.0[(a)], 6.34[(e)]		5.9	− 14.23

agreement between our measured broadenings and existing measured and calculated values can be observed in Table II and Fig. 3. Especially, values of the line broadening retrieved in this work using the qSDHC model lead to the best agreement with those obtained by close-coupling calculations.[36]

III. CLASSICAL MOLECULAR DYNAMICS SIMULATIONS

A. Calculations procedure

CMDS[37] have been performed for the mixture of HCl-Ar at room temperature and a density of 2.5 amagat. The HCl molecule is described by the three-site model of Ref. 38. Only the $H^{35}Cl$ isotope has been considered. The anisotropic atom-diatom Lennard-Jones potential SSP of Ref. 39 has been used to represent the interactions between HCl and Ar. A Lennard-Jones potential with parameters from Ref. 40 is used for Ar-Ar. For HCl-HCl, the potential contains two terms. The first one is a columbic site-site interaction with the charges and distances between sites given in Ref. 38. The second term is an atom-atom anisotropic potential with parameters deduced from those of HCl-Ar and Ar-Ar using usual combination rules for binary mixtures.

The molecules and atoms are initially randomly placed inside 200 cubic boxes with periodic boundary conditions; each box contains 2×10^4 molecules leading to a total of 4×10^6 molecules and atoms. The initial distance between the particles has been imposed to be larger than 15 Å in order to avoid unphysical situations involving strong intermolecular interaction at time zero. For the translational velocity and angular velocity (for HCl molecules), Boltzmann distributions have been randomly attributed to their modulus while random values have been chosen for their orientation. At each time step, the force and the torque applied to each particle by its neighbors are computed. The translational velocity $\vec{v}_i(t)$, the angular velocity $\vec{\omega}_i(t)$ and hence the center-of mass position $\vec{r}_i(t)$ and the molecular orientation (characterized by the unit vector $\vec{u}_i(t)$ along the molecule axis) are then determined at each time step. A temporization time has been observed in order to ensure that the initial configuration is completely thermalized.[37]

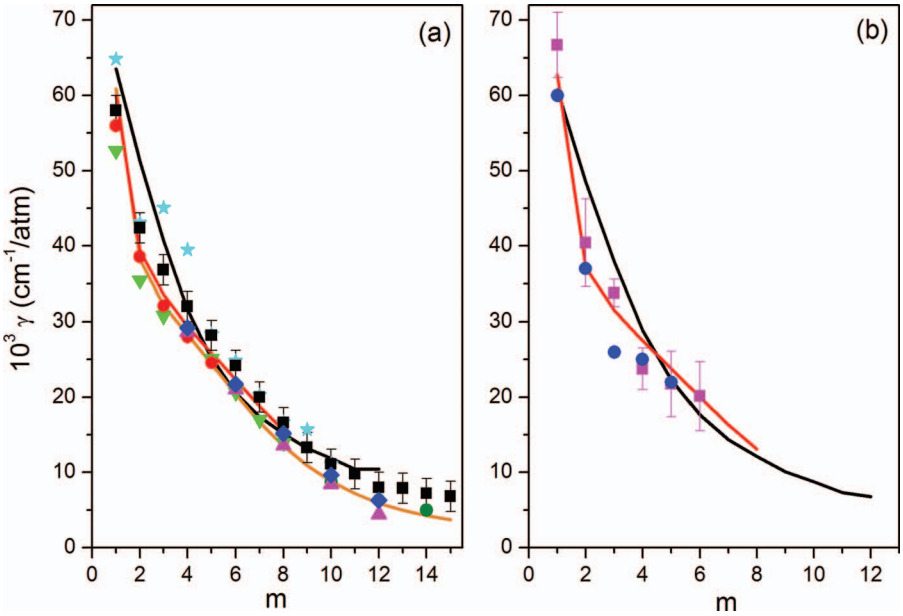

FIG. 3. (a) Ar broadening coefficient of HCl lines in the R branch of the 1-0 band. The black, orange, and red lines are the calculated values obtained by the present CMDS (see text), the Neilson and Gordon classical formalism[35] and by close-coupling calculations,[36] respectively. The symbols are the measured values of the present work using Voigt profiles (magenta triangles) and the qSDHC profile (blue diamonds) to fit the measured spectra. Measured values of Refs. 52 (cyan stars),[51] (green triangles),[53] (red circles),[4] (olive full circle), and Ref. 35 (black squares) are also reported for comparison. (b) Ar broadening coefficient of HCl lines in the R branch of the pure rotation band. In the black and red lines are computed values resulted from CMDS of this work and from CC calculation by Ref. 36. In squared-magenta and circled-blue symbols are represented the measured values of Ref. 54 and of Refs. 55 and 56, respectively.

In order to compute a spectrum with line structure by CMDS, a requantization procedure of the classical rotational angular momentum has to be performed. As the rotational constant of HCl is relatively large (i.e., about 10.44 cm^{-1} in the fundamental vibrational state[41]), the requantization procedure as done in Refs. 19 and 20 for CO_2 and O_2 cannot be applied here. In that procedure, the modulus of the classical rotational angular velocity ω_i was requantized in order to match the closest rotational quantum number J_i. In other words, the value of ω_i is (slightly) changed such that the classical rotational energy ($\frac{1}{2}I\omega_i^2$) is equal to that of the corresponding rotational quantum level ($\frac{J_i(J_i+1)\hbar^2}{2I}$) with I the moment of inertia. This requantization was applied only when the torque due to intermolecular interactions is below a properly chosen limit in order to let rotational-speed changes build up during collisions.[19,20] Thanks to the small values of the rotational constants of CO_2 and O_2, the changes of ω_i induced by this requantization do not influence the evolution of the system and its energy is thus conserved. For HCl which has a much larger rotational constant, a new requantization scheme has been used.

In this new approach, one considers the angle $\theta_i(t)$ between the unit vectors along the molecule axis at time zero, $\vec{u}_i(0)$, and at time t, $\vec{u}_i(t)$. This angle is calculated for each time step by

$$\theta_i(t+dt) = \left\{\theta_i(t) + \text{sign}\omega_i^{req}(t)dt\right\}\cos[\vec{u}_i(t), \vec{u}_i(0) \times \vec{u}_i(t+dt)], \quad (1)$$

where ω_i^{req} is the requantized value of the classical rotational angular velocity ω_i, i.e.: $\vec{\omega}_i^{req} = \vec{\omega}_i \frac{\sqrt{J_i(J_i+1)}\hbar/I}{\|\vec{\omega}_i\|}$ with J_i the corresponding quantum level. In Eq. (1), sign is the sign of the projection of the vector product of the rotational angular velocity $\vec{\omega}_i$ and the molecular axis $\vec{u}_i(t)$ along the fixed axis x.[42,43] $\theta_i(t)$ and thus the auto-correlation function of the dipole moment (carried by the molecular axis) are then calculated for each time step using this requantization procedure. The other parameters such as $\vec{\omega}_i$, $\vec{u}_i(t)$ are kept unchanged with respect to their classical values and follow the classical evolution of the system. The requantization procedure is thus applied only to the computed auto-correlation function of the dipole moment as a post-treatment of the CMDS results and thus does not influence the classical evolution of the system. With this new scheme, one can thus compute the spectrum of HCl with a line structure and ensure the normal evolution of the system.

B. Results of CMDS

CMDS have been performed from the initial time to up to 1500 ps with a time step of about 0.8 fs. Since the temperatures computed from the average translational or rotational energies remain unchanged throughout the calculation, no correction was applied.

First, the auto-correlation function of various translational-velocity-related quantities has been computed by CMDS, e.g., for the translation velocity:

$$\Phi_{\vec{v}}(t) = \langle\vec{v}(t).\vec{v}(0)\rangle = \frac{1}{N_M}\sum_{i=1,N_M}\vec{v}_i(t).\vec{v}_i(0), \quad (2)$$

with N_M the total number of HCl molecules. Figure 4 presents the computed auto-correlation functions of the translational velocity $\Phi_{\vec{v}}(t)$, of the translational speed $\Phi_v(t)$,

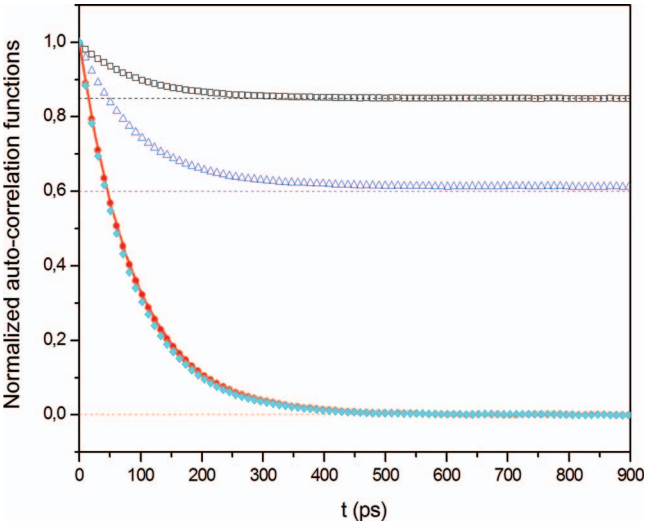

FIG. 4. Normalized auto-correlation functions of the translational velocity $\Phi_{\vec{v}}(t)$ (red circles), of the translational speed $\Phi_{v}(t)$ (black squares), of the squared-speed $\Phi_{v^2}(t)$ (blue triangles), and of the velocity orientation $\Phi_{\vec{v}/\|\vec{v}\|}(t)$ (cyan diamonds) of HCl infinitely diluted in Ar, computed at 296 K and 2.5 amagat. The dashed lines indicate the $t \rightarrow \infty$ theoretical limits[44] of these ACFs while the red solid line is the exponential decay fit of $\Phi_{\vec{v}}(t)$.

of the squared-speed $\Phi_{v^2}(t)$ and of the velocity orientation $\Phi_{\vec{v}/\|\vec{v}\|}(t)$. These functions are normalized by their corresponding values at time zero, deduced from Boltzmann statistics.[44] The expected values at $t \rightarrow \infty$, also deduced from Boltzmann statistics,[44] are plotted for comparison with CMDS results where a good agreement can be observed.

From the time constant, $\tau_{\vec{v}}$, of the exponential decay of the translational-velocity auto-correlation function, the corresponding mass diffusion coefficient can be directly deduced, i.e., $D = \frac{\tau_{\vec{v}} k_B T}{m}$ where m is the molecular mass and k_B is the Boltzmann constant. As can be observed in Fig. 4, the auto-correlation function of HCl in Ar can be nicely fitted by an exponential decay function. The deduced time constant $\tau_{\vec{v}}$ is 226.75 ps at 1 amagat, leading to a mass diffusion coefficient of HCl in Ar, $D_{HCl\text{-}Ar}$, of 0.141 $cm^2\ s^{-1}$ at 1 atm and 296 K. This value is in good agreement with that, of 0.140 $cm^2\ s^{-1}$, deduced from observed line widths of HCl in Ar using diffusion theory[4] and of 0.152 $cm^2\ s^{-1}$, value calculated from measured self-diffusion coefficients for HCl and Ar.[45] These results thus provide a first validation of the present CMDS.

The auto-correlation function of the molecular dipole of HCl molecule, $\vec{d}(t)$, including the Doppler effect, is com-

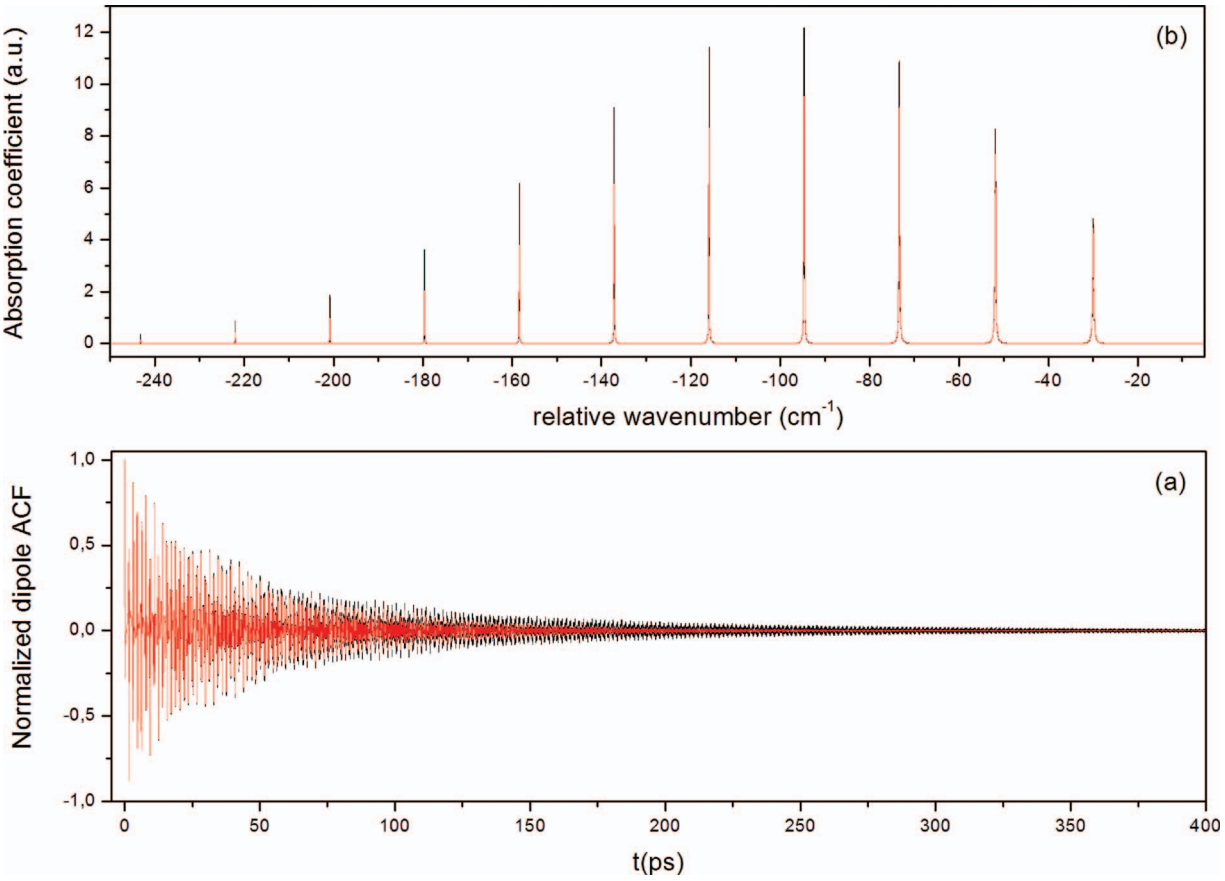

FIG. 5. (Lower panel) Normalized (at $t = 0$) dipole auto-correlation functions computed by CMDS for HCl infinitely diluted in Ar at 296 K and 2.5 amagat without Doppler contribution (black line) and with a Doppler contribution corresponding to wave number of $\omega_0/2\pi c = 58\,000\ cm^{-1}$ (red line). In the upper panel is a portion (in the P branch region) of the corresponding spectra.

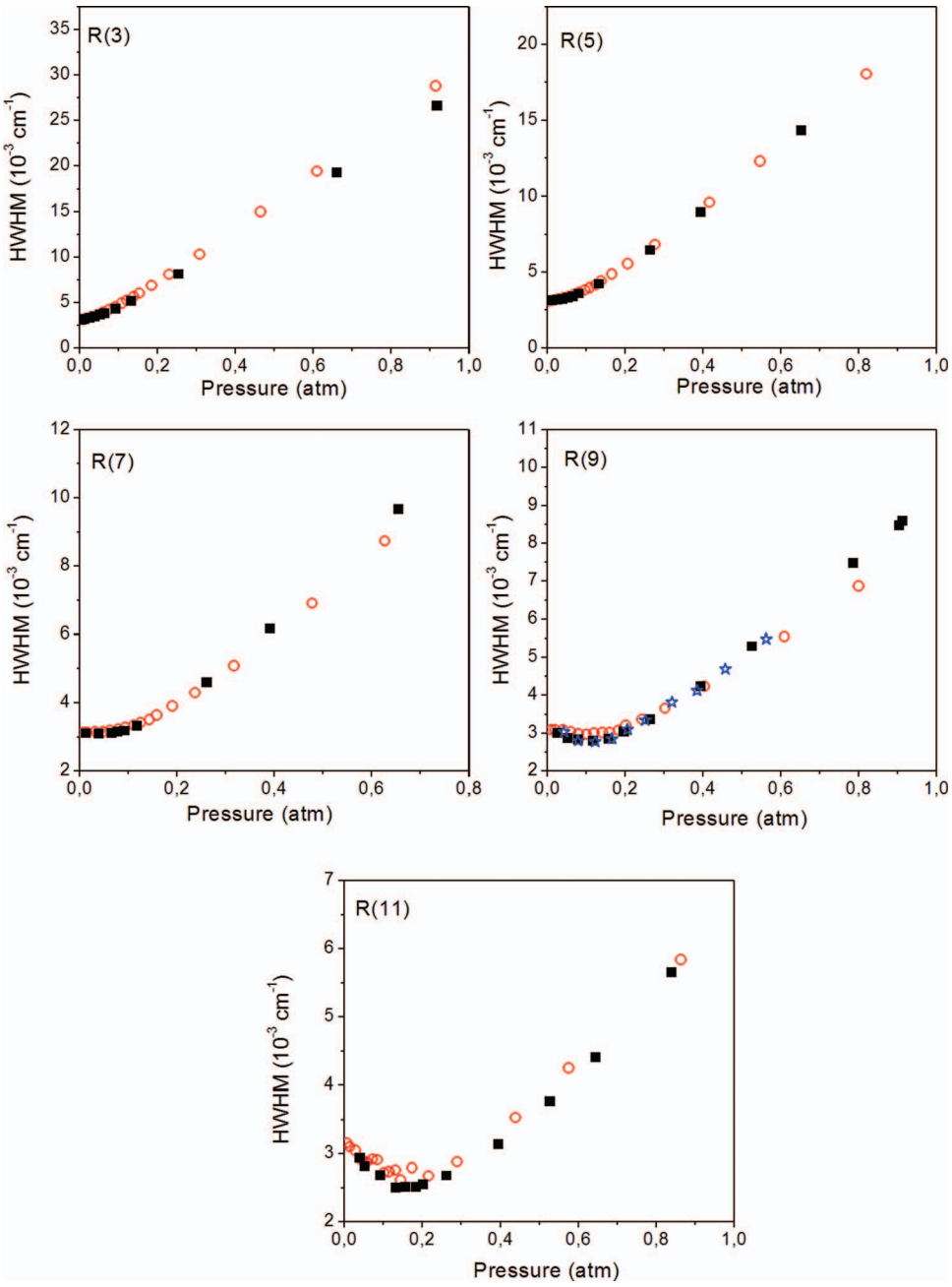

FIG. 6. Comparison between room temperature measured (black squares) and CMDS-computed (red circles) apparent HWHM (half-width at half-maximum) of HCl infinitely diluted in Ar for all considered lines. Measured values of Ref. 4 (blue stars) for the R(9) lines are also reported.

puted by CMDS. For a dipole vector carried by the molecular axis $\vec{u}(t)$, the normalized dipole auto-correlation function is given by[19]

$$\Phi(t) = \frac{1}{N_M} \sum_{i=1,M} e^{-i\vec{k}[\vec{r}_i(t)-\vec{r}_i(0)]} [\vec{u}_i(t).\vec{u}_i(0)]$$
$$= \frac{1}{N_M} \sum_{i=1,M} e^{-i\vec{k}[\vec{r}_i(t)-\vec{r}_i(0)]} \cos[\theta_i(t)], \quad (3)$$

where $\vec{k} = (\omega_0/c)\vec{z}$ is the wave vector and the exponential term is related to the Doppler effect associated with the translational motion. The angle $\theta(t)$ between $\vec{u}(t)$ and $\vec{u}(0)$ is computed at each time step using the requantized rotational angular velocity ω_i^{req} as explained in Sec. III A. The time evolution of $\Phi(t)$ is thus easily computed from the values of $\theta(t)$ and $\vec{r}(t)$. The normalized absorption coefficient at angular frequency ω is then directly obtained from the Fourier-Laplace transform of $\Phi(t)$, i.e.,[19,46]

$$F(\omega) = \mathrm{Re}\left\{ \frac{1}{\pi} \int_0^\infty \Phi(t) e^{-i\omega t} dt \right\}. \quad (4)$$

Examples of normalized auto-correlation functions of the dipole moment and the corresponding spectra are given in Figs. 5(a) and 5(b), respectively.

From the CMDS theoretical spectrum computed without any Doppler contribution (only the collisional effect is taken into account), the collisional line widths are deduced by fitting this spectrum with Lorentzian profiles. The obtained CMDS-computed collisional broadenings are plotted in Fig. 3(b). They are compared with values measured and calculated for the rotational band of HCl since no vibrational contribution has been taken into account in our CMDS. As can be observed, the CMDS-computed broadenings are in rather good agreement with CC-calculated values as well as with measured ones. Note that the available experimental values of γ in the pure rotation spectrum having been measured in the seventies, new and more accurate measurement for a larger range of the rotational quantum number will allow a better test of the calculation. The remaining differences between CMDS- and CC-calculated broadenings are probably due to the classical treatment of the rotation of the HCl molecule. They could also be due to the simple intermolecular potential used in this work.

In order to take into account the vibrational contribution in the CMDS-computed spectra, a more accurate intermolecular potential which includes the dependence on the vibrational state of HCl should be used. Meanwhile, in the present work, we have chosen to introduce an effective term which represents the vibrational contribution. In this case, the normalized absorption coefficient of Eq. (4) becomes

$$F(\omega) = \mathrm{Re}\left\{\frac{1}{\pi}\int_0^\infty \Phi(t)e^{-i\omega t}e^{-\Gamma_{vib}t}dt\right\}, \quad (5)$$

with Γ_{vib} is a vibrational width, assumed independent of the molecular speed. Note that the vibrational dephasing contribution leading to a vibrational shift was neglected. A value of $\Gamma_{vib} = 2.7 \times 10^{-3}$ cm^{-1}/atm at room temperature was deduced from the broadening coefficients computed for the pure rotational, the first and second overtone bands of HCl by the CC method.[36] The final Lorentzian broadening coefficient in the 1-0 band, computed from CMDS and taking into account the vibrational contribution by this empirical method are then compared with measured values in Fig. 3(a) where a good agreement with existing measured and calculated values can be observed. The corresponding spectral profiles are compared with measured spectra in Sec. IV.

IV. COMPARISON BETWEEN MEASURED AND CMDS-CALCULATED SPECTRAL PROFILES

The total half-widths at half-maximum (HWHM) of the measured and CMDS-calculated spectra versus pressure are first compared. For that, CMDS calculations have been performed for 20 values of the Doppler width [from 3.119 $\times 10^{-3}$ to 1.185 cm^{-1}, by varying the Doppler contribution in Eq. (3)]. For a given transition, the comparison has been done using the "equivalent pressure," deduced from the density (2.5 amagat) and the temperature (296 K) used in the calculations. This "equivalent pressure" is equal to the product of the pressure used in the calculation by the ratio of the measured Doppler width to the calculated Doppler width. The calculated HWHM, also multiplied by this ratio, is then compared with the HWHM of the corresponding measured line.

Figure 6 shows the comparison between the measured and calculated HWHM versus Ar pressure for all considered lines. As for the collisional line width, the HCl self-broadening contribution has been subtracted from the total measured HWHM. Experimental and calculated conditions have been chosen such that the Dicke minimum of each considered line is covered both by the measurement and the calculation. As can be observed in Fig. 6, with respect to the Doppler width, the Dicke minimum becomes more pronounced for increasing rotational quantum number. This means that for HCl-Ar interactions, velocity-changing collisions are very efficient and that for high rotational quantum numbers, they are predominant with respect to internal-state-changing collisions. For all considered lines, a very good agreement between the CMDS-calculated and measured HWHMs is obtained. They are also in good agreement with previous measurements of Ref. 4. Note that the scatter observed in the CMDS results for the R(11) line is due to the numerical noise of our CMDS calculations. The R(11) line is very weak [more than two orders of magnitude weaker than the R(3) line], so a much larger number of molecules is necessary to ensure a good signal-to-noise ratio in its calculated absorption spectrum.

Comparisons between measured and CMDS-calculated spectra have been also made using their fits with the Voigt

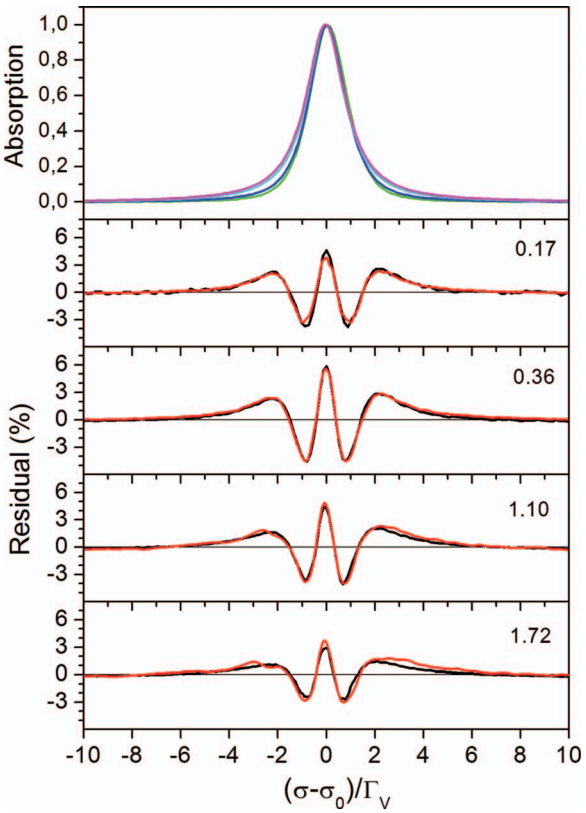

FIG. 7. Normalized absorptions (top panel) of the R(7) line, measured at various pressures and residuals obtained from fits with the Voigt profile of these measured spectra (black lines) and of CMDS-calculated spectra (red lines), the number in each panel being the corresponding Lorentz to Doppler widths (Γ_L/Γ_D) ratio.

profile as done previously for CO_2 and O_2.[19–22] For that, all measured and calculated spectra have been fitted with Voigt profiles, and we then compare the obtained fit residuals and retrieved parameters. This allows another comparison between measured and calculated spectra. Figure 7 presents an example of residuals obtained from fit of measured and calculated spectra by Voigt profiles for the R(7) line for different Lorentz-to-Doppler widths (Γ_L/Γ_D) ratios (i.e., different pressures). Each spectrum and its fit residual are plotted versus the relative wavenumber normalized by the estimated Voigt width.[47] As can be observed in Fig. 7, a very good agreement between the residuals is obtained for all considered values of Γ_L/Γ_D. The amplitude (W) of these Voigt-fit residuals (maximum minus minimum values of the W-shape residual as observed in Fig. 7) is plotted for all considered lines in Fig. 8 except the R(11) line for which non-Voigt effects are so large that, at low and intermediate pressures, the spectra cannot be fitted with the Voigt profile. The evolution of the retrieved Lorentz broadening coefficients with Γ_L/Γ_D is also plotted in this figure. Note that for each considered line, a multiplicative factor (close to 1) was applied to the broadening coefficient obtained from CMDS-calculated spectra in order to match the measured one at high values of Γ_L/Γ_D.

As can be observed in Fig. 8, the amplitude of the residuals has the same evolution versus Γ_L/Γ_D for all considered lines: W first increases with Γ_L/Γ_D when Γ_L/Γ_D is small, it then reaches a maximum value and finally decreases when Γ_L/Γ_D increases. This evolution of W with Γ_L/Γ_D has already been observed for other molecular systems.[19–21,48–50] On the opposite, the value of W strongly depends on the line, W being larger for high rotational quantum numbers, in consistency with the results of Fig. 6 where deeper Dicke minima are observed for high J. For all considered lines, the values of W deduced from CMDS calculations are in very good agreement with those obtained from measured spectra. A good agreement is also obtained for the Lorentz broadening coefficients retrieved from CMDS-calculated and measured spectra.

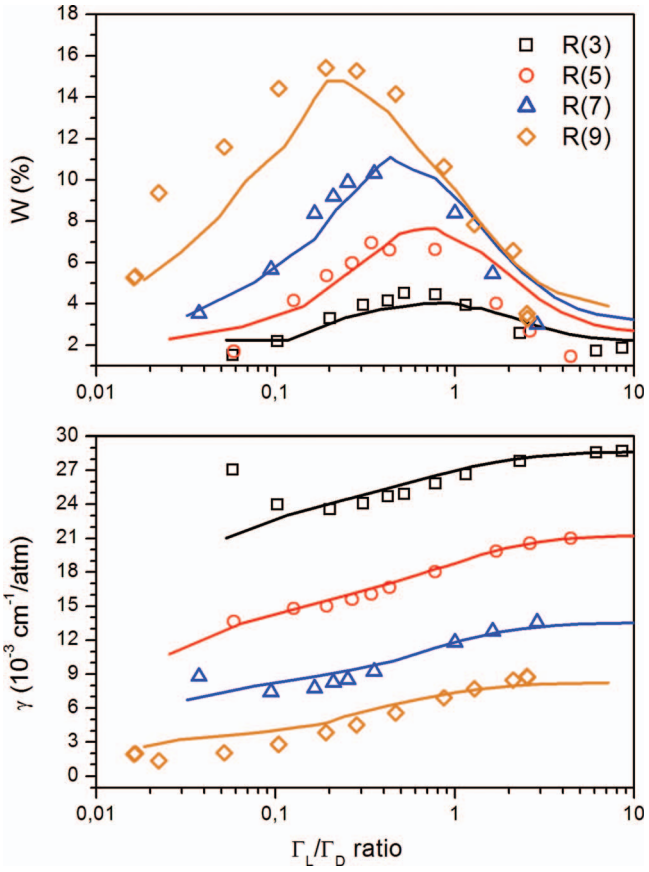

FIG. 8. Peak-absorption-normalized amplitude of the residuals (upper panel) and broadening coefficients (lower panel) obtained from fit of measured and CMDS-calculated spectra with Voigt profiles for all considered lines, versus the Lorentz to Doppler (Γ_L/Γ_D) ratio. Lines are results obtained from CMDS-calculated spectra while results obtained from measured spectra are plotted in symbols.

V. CONCLUSIONS

Spectral shapes of isolated lines of HCl perturbed by Ar have been investigated for the first time using classical molecular dynamics simulations. Using intermolecular potentials taken from literature, CMDS provide the time evolution of the auto-correlation function of the dipole moment, whose Fourier-Laplace transform leads to the absorption spectrum. The spectral shapes of several isolated lines of HCl in Ar have been computed by these *ab initio* calculations. The computed spectra have been successfully compared with high resolution spectra of HCl in Ar, measured by a difference-frequency laser spectrometer. Comparisons between measured and calculated spectra have shown that CMDS calculations are able to predict the large Dicke narrowing effect on the shape of HCl lines and to satisfactorily reproduce HCl line shapes at different pressures and for various rotational quantum numbers. These CMDS, now fully validated, can thus be used to analyze the relative contributions of different non-Voigt effects (velocity changes, speed-dependence of the line width and shift, correlation between velocity and internal-state changes) to the line shape of HCl. This will be performed in a forthcoming study. Furthermore, CMDS can also be extended to compute HCl spectra at high pressures for which no theoretical modeling successfully explains the behavior of the spectra in the far wings.[46]

ACKNOWLEDGMENTS

H. Tran thanks the *Institut du Développement et des Ressources en Informatique Scientifique* (IDRIS) for giving access to the IBM Blue Gene/Q parallel computer. J.-L. Domenech acknowledges the financial support of MINECO through grants Consolider CSD2009-00038 (Astromol) and FIS2012-38175. J.-M. Hartmann is gratefully acknowledged for helpful discussions.

[1]G. H. Wegdam and A. H. M. Sondag, Chem. Phys. Lett. **111**, 360 (1984).
[2]A. S. Pine and A. Fried, J. Mol. Spectrosc. **114**, 148 (1985).
[3]A. S. Pine and J. P. Looney, J. Mol. Spectrosc. **122**, 41 (1987).
[4]D. R. Rao and T. Oka, J. Mol. Spectrosc. **122**, 16 (1987).
[5]A. Henry and D. Hurtmans, Spectrochim. Acta, Part A **55**, 1967 (1999).
[6]I. Morino and K. M. T. Yamada, J. Mol. Spectrosc. **233**, 77 (2005).
[7]D. Hurtmans, A. Henry, A. Valentin, and C. Boulet, J. Mol. Spectrosc. **254**, 126 (2009).
[8]M. Nelkin and A. Ghatak, Phys. Rev. **135**, A4 (1964).
[9]S. G. Rautian and I. I. Sobel'man, Sov. Phys. Usp. **9**, 701 (1967).

[10]L. Galatry, Phys. Rev. **122**, 1218 (1961).
[11]B. Barret, D. Hurtmans, M. R. Carleer, M. De Mazière, E. Mahieu, and P.-F. Coheur, J. Quant. Spectrosc. Radiat. Transfer **95**, 499 (2005).
[12]A. S. Pine, J. Chem. Phys. **101**, 3444 (1994).
[13]A. S. Pine, J. Quant. Spectrosc. Radiat. Transfer **62**, 397 (1999).
[14]J. Ward, J. Cooper, and E. W. Smith, J. Quant. Spectrosc. Radiat. Transfer **14**, 555 (1974).
[15]P. R. Berman, J. Quant. Spectrosc. Radiat. Transfer **12**, 1331 (1972).
[16]P. Duggan, P. M. Sinclair, A. D. May, and J. R. Drummond, Phys. Rev. A **51**, 218 (1995).
[17]A. Henry, D. Hurtmans, M. Margottin-Maclou, and A. Valentin, J. Quant. Spectrosc. Radiat. Transfer **56**, 647 (1996).
[18]R. Ciurylo, A. S. Pine, and J. Szudy, J. Quant. Spectrosc. Radiat. Transfer **68**, 257 (2001).
[19]J.-M. Hartmann, H. Tran, N. H. Ngo, X. Landsheere, P. Chelin *et al.*, Phys. Rev. A **87**, 013403 (2013).
[20]J.-M. Hartmann, V. Sironneau, C. Boulet, T. Svensson, J. T. Hodges, and C. T. Xu, Phys. Rev. A **87**, 032510 (2013).
[21]G. Larcher, H. Tran, M. Schwell, P. Chelin, X. Landsheere, J.-M. Hartmann, and S.-M. Hu, J. Chem. Phys. **140**, 084308 (2014).
[22]J. Lamouroux, V. Sironneau, J. T. Hodges, and J.-M. Hartmann, Phys. Rev. A **89**, 042504 (2014).
[23]A. S. Pine, J. Opt. Soc. Am. **66**, 97 (1976).
[24]J. L. Domenech, D. Bermejo, J. Santos, J. P. Bouanich, and C. Boulet, J. Mol. Spectrosc. **169**, 211 (1995).
[25]T. J. Quinn, Metrologia **40**, 103 (2003).
[26]F. Rohart, H. Mader, and H.-W. Nicolaisen, J. Chem. Phys. **101**, 6475 (1994).
[27]F. Rohart, A. Ellendt, F. Kaghat, and H. Mäder, J. Mol. Spectrosc. **185**, 222 (1997).
[28]B. Lance, G. Blanquet, J. Walrand, and J.-P. Bouanich, J. Mol. Spectrosc. **185**, 262 (1997).
[29]D. Lisak, D. K. Havey, and J. T. Hodges, Phys. Rev. A **79**, 052507 (2009).
[30]D. A. Long, K. Bielska, D. Lisak, D. K. Havey, M. Okumura, C. E. Miller, and J. T. Hodges, J. Chem. Phys. **135**, 064308 (2011).
[31]N. H. Ngo, D. Lisak, H. Tran, and J.-M. Hartmann, J. Quant. Spectrosc. Radiat. Transfer **129**, 89 (2013).
[32]H. Tran, N. H. Ngo, and J.-M. Hartmann, J. Quant. Spectrosc. Radiat. Transfer **129**, 199 (2013).
[33]M. Abramowitz and I. A. Stegun, *Handbook of Mathematical Functions with Formulas, Graphs, and Mathematical Tables* (Dover Publications, New York, 1972).
[34]L. S. Rothman, I. E. Gordon, Y. Babikov, A. Barbe, D. Chris Benner *et al.*, J. Quant. Spectrosc. Radiat. Transfer **130**, 4 (2013).
[35]C. Boulet, P.-M. Flaud, and J.-M. Hartmann, J. Chem. Phys. **120**, 11053 (2004).
[36]C. F. Roche, J. M. Hutson, and A. S. Dickinson, J. Quant. Spectrosc. Radiat. Transfer **53**, 153 (1995).
[37]M. P. Allen and D. J. Tildesley, *Computer Simulation of Liquids* (Clarendon, Oxford, 1987).
[38]A. Laaksonen and P. O. Westlund, Mol. Phys. **73**, 663 (1991).
[39]A. Medina, J. M. M. Roco, A. Calvo Hernandez, and S. Velasco, J. Chem. Phys. **121**, 6353 (2004).
[40]P. N. M. Hoang, P. Joubert, and D. Robert, Phys. Rev. A **65**, 012507 (2001).
[41]D. H. Rank, D. P. Eastman, B. S. Rao, and T. A. Wiggins, J. Opt. Soc. Am. **52**, 1 (1962).
[42]J. Lamouroux, J.-M. Hartmann, H. Tran, B. Lavorel, M. Snels, S. Stefani, and G. Piccioni, J. Chem. Phys. **138**, 244310 (2013).
[43]R. G. Gordon, J. Chem. Phys. **45**, 1649 (1966).
[44]H. Tran, J.-M. Hartmann, F. Chaussard, and M. Gupta, J. Chem. Phys. **131**, 154303 (2009).
[45]Landolt-Bornstein, *Landolt-Bornstein Zahlenwerte und Funktionen* (Springer, Berlin, 1960).
[46]J.-M. Hartmann, C. Boulet, and D. Robert, *Collisional Effects on Molecular Spectra. Laboratory Experiments and Models, Consequences for Applications* (Elsevier, Amsterdam, 2008).
[47]J. J. Olivero and R. L. Longbothum, J. Quant. Spectrosc. Radiat. Transfer **17**, 233 (1977).
[48]H. Tran, D. Bermejo, J.-L. Domenech, P. Joubert, R. R. Gamache, and J.-M. Hartmann, J. Quant. Spectrosc. Radiat. Transfer **108**, 126 (2007).
[49]N. H. Ngo, H. Tran, and R. R. Gamache, J. Chem. Phys. **136**, 154310 (2012).
[50]N. H. Ngo, H. Tran, R. R. Gamache, D. Bermejo, and J.-L. Domenech, J. Chem. Phys. **137**, 064302 (2012).
[51]A. Levy, E. Piollet-Mariel, and C. Boulet, J. Quant. Spectrosc. Radiat. Transfer **13**, 673 (1973).
[52]D. H. Rank, D. P. Eastman, B. S. Rao, and T. A. Wiggins, J. Mol. Spectrosc. **10**, 34 (1963).
[53]J. P. Houdeau and C. Boulet, J. Quant. Spectrosc. Radiat. Transfer **26**, 503 (1981).
[54]R. M. van Aalst, J. A. Schuurman, and J. van der Elsken, Chem. Phys. Lett. **35**, 558 (1975).
[55]H. A. Gebbie and N. W. B. Stone, Proc. Phys. Soc. **82**, 309 (1963).
[56]M. Giraud, D. Robert, and L. Galatry, J. Chem. Phys. **53**, 352 (1970).